Available online at www.sciencedirect.com
SCIENCE DIRECT®
PERGAMON
Deep-Sea Research I 50 (2003) 53–71
DEEP-SEA RESEARCH PART I
www.elsevier.com/locate/dsr

Vertical diffusion and oxygen consumption during stagnation periods in the deep North Aegean

Vassilis Zervakis*, Evangelia Krasakopoulou, Dimitris Georgopoulos, Ekaterini Souvermezoglou

National Centre for Marine Research, GR-16604 Aghios Kosmas, Hellinikon, Greece

Received 26 February 2002; received in revised form 8 October 2002; accepted 19 October 2002

Abstract

Ventilation of the deep basins of the North Aegean Sea takes place during relatively scarce events of massive dense water formation in that region. In the time intervals between such events, the bottom waters of each sub-basin are excluded from interaction with other water masses through advection or isopycnal mixing and the only process that changes their properties is diapycnal mixing with overlying waters. In this work we utilize a simple one-dimensional model in order to estimate the vertical eddy diffusion coefficient K_ρ based on the observed rate of change of density and stratification. Vertical diffusivity is estimated for each of three sub-basins of the North Aegean, one of convex shape of the seabed and the other two of concave topography. It is noteworthy that the convex sub-basin exhibited much higher vertical diffusivity than the two concave sub-basins, a fact consistent with theoretical predictions that internal-wave-induced mixing is higher over the former shape of seabed. Furthermore, the estimates of K_ρ are exploited in computing the vertical transport of dissolved oxygen through diffusion and the rate of oxygen consumption by decaying organic matter. The different levels of the estimated diffusion and oxygen consumption rates testify to the dynamical and biogeochemical characteristics of each basin.

Keywords: Mixing processes; Eddy diffusivity; Oxygen consumption; Vertical mixing; Eastern Mediterranean; Aegean Sea

1. Introduction

The North Aegean Sea is the region of the Mediterranean Sea where Black Sea waters enter through the Dardanelles Straits. The Black Sea exchanges water with the Mediterranean through a two-layer flow along the straits system comprised of the strait of Dardanelles, the Marmara Sea and the strait of Bosphorus (Fig. 1). As the Black Sea is (contrary to the Mediterranean) a dilution (estuarine) basin, characterized by surface salinities less than 20, the surface layer at the Straits flows towards the highly saline Mediterranean ($S > 38$), and the subsurface layer towards the Black Sea. This flow is hydraulically controlled, and as a result of the increased mixing along the Straits, the salinity at the Aegean exit of the Dardanelles reaches about 28 (Ünlüata et al., 1990). Still, the salinity difference with the surrounding Aegean waters causes such a density difference that the

*Corresponding author. Tel.: +30-2910-76402; fax: +30-2910-76323.
E-mail address: zervakis@ncmr.gr (V. Zervakis).

0967-0637/03/$ - see front matter
PII: S0967-0637(02)00144-9

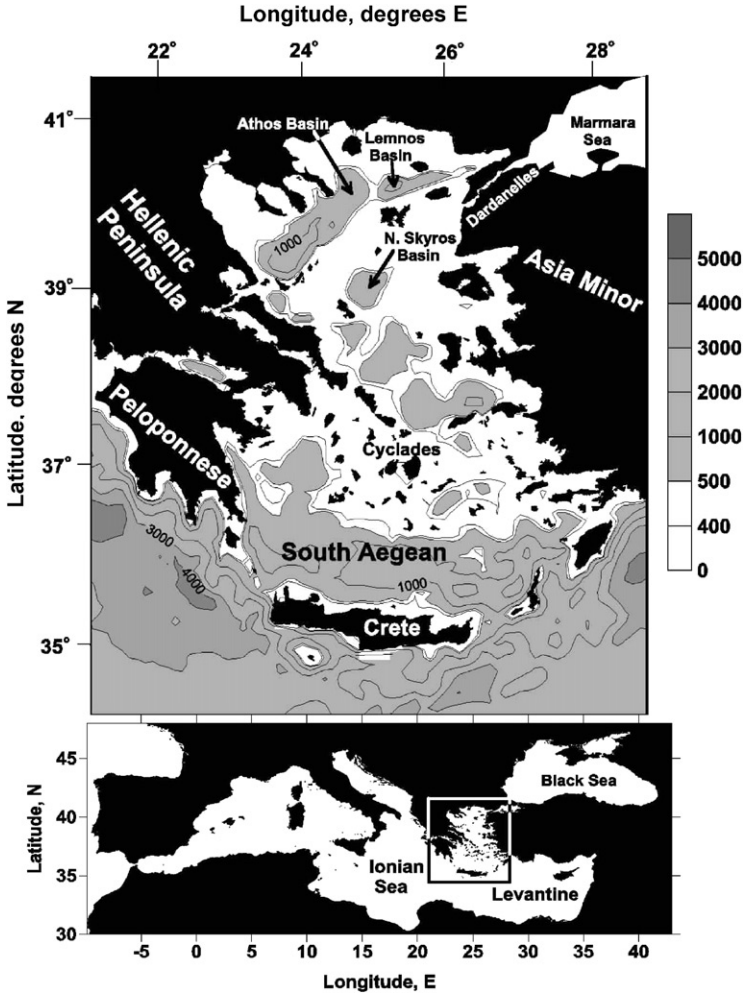

Fig. 1. The Aegean Sea geography and bathymetry. The depths deeper than 500 m are shaded. Isobaths of 400, 500, 1000, 2000, 3000 and 4000 m are shown. The Athos–North Sporades, Lemnos and North Skyros basins of the North Aegean referred to in the text are identified. The box in the map of the Mediterranean provided below shows the position of the Aegean Sea.

modified Black Sea water (hereafter referred to as BSW) plume generates a thin (about 20 m) surface layer that covers the majority of the North Aegean (Zodiatis, 1994).

The North Aegean is included in many studies as one of the regions of bottom water formation of the Mediterranean (Nielsen, 1912; Plakhin, 1972; Theocharis and Georgopoulos, 1993; Zervakis et al., 2000). It is one of the northern extremities of the Mediterranean, like the Gulf of Lions and the Northern Adriatic, both sources of bottom water (Nielsen, 1912; Pollak, 1951; Stommel, 1972). Indeed, the deep sub-basins of the North Aegean, separated from each other and from the South Aegean by 350–400 m deep shelves and sills, are filled with extremely dense water, with recorded potential density exceeding $\sigma_\theta = 29.63\,\mathrm{kg\,m^{-3}}$ (Zervakis et al., 2000). The communication between the North and South Aegean is free above the 400 m isobath, and thus the intermediate layer of the North Aegean is filled with water of Levantine origin. Above the

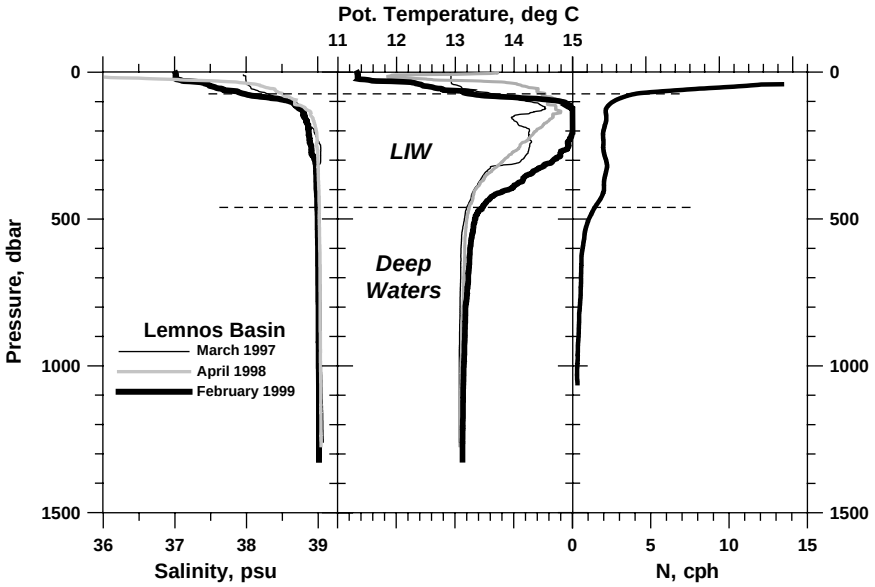

Fig. 2. Vertical profiles of salinity (left), temperature (middle) and average buoyancy frequency (right) in Lemnos basin. The dashed lines identify the approximate position of the interfaces separating the three layers of the North Aegean.

intermediate layer lies a surface layer containing modified Black Sea water, thus characterized by low salinity (Fig. 2).

The fact that the deep waters of the South Aegean are much lighter than those of the North Aegean certifies that the latter are locally formed. In a study of the evolution of the North Aegean water columns through the late 1980s/early 1990s, Zervakis et al. (2000) showed that incidents of local formation of very dense waters in the North Aegean took place in the winters of 1987 and 1992/1993 (Fig. 3). Furthermore, they showed evidence that the deep water formation incidents coincided with periods of reduced water surplus of the Black Sea, thus a weaker surface layer of BSW in the North Aegean. Zervakis et al. (2000) suggested that the surface layer of the North Aegean is an effective isolator between the deep layers of the North Aegean and the atmosphere, absorbing large amounts of heat and buoyancy and hindering dense water formation. Thus, they show that dense water formation events in the North Aegean demand not only large exchange of buoyancy with the atmosphere (the winter of 1987 was one of the coldest of the century in the region and the period 1992–1993 very dry), but also a significant reduction of the surface isolation lid, thus a reduction of the water surplus of the Black Sea.

This combination of factors necessary for deep water formation in the North Aegean reduces the frequency with which such events take place. Indeed, all evidence suggests that there has been no ventilation of the deep waters of the North Aegean in the period from 1994 to 2000. The time periods between events of bottom water formation are called stagnation periods; 1994–2000 has been a long stagnation period in the North Aegean. Successive cruises in the region in the period 1997–2000 have provided us with data showing a gradual decrease of the deep-layer density and dissolved oxygen (Fig. 4). This work utilizes a one-dimensional conceptual model to explain the gradual decrease of density and dissolved oxygen in the secluded from advection deep basins of the North Aegean.

2. Data sampling

Two multidisciplinary projects that took place simultaneously from 1997 to 2000 gave NCMR the opportunity to perform repetitive sampling in the

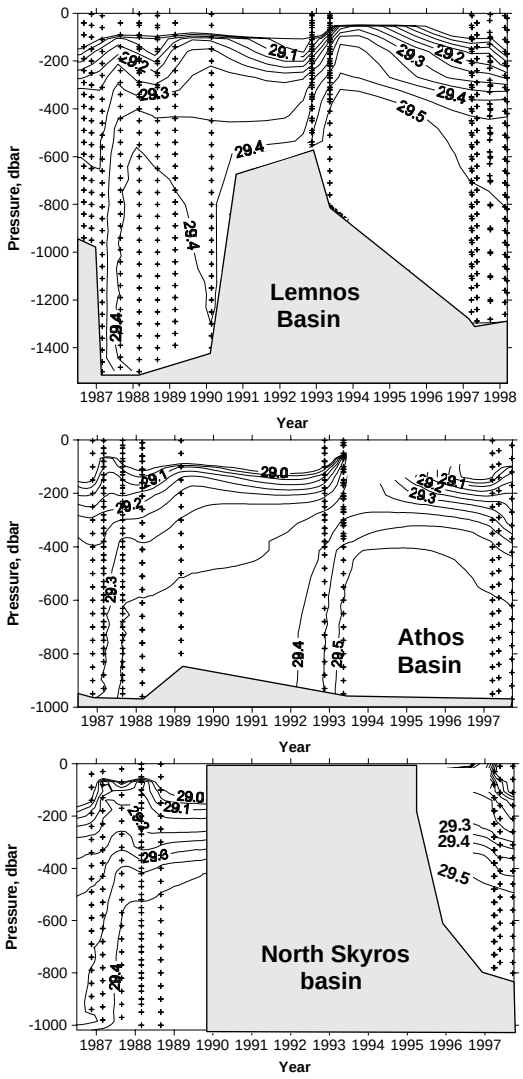

Fig. 3. Density (σ_θ) contours versus time and depth showing the evolution of the pycnocline between 1986 and 1998 in the three basins of the North Aegean (figure from Zervakis et al., 2000). Shaded regions denote lack of data.

deep basins of the North Aegean. The MTP-II MATER program, funded by the European Commission, aimed to describe the biogeochemical cycles in the Mediterranean, while a nationally funded project through the INTERREG program studied interregional pollution in the North Aegean Sea. The θ/S properties of the water were recorded with a Seabird Electronics SBE-911+ CTD attached to a General Oceanics rosette sampler equipped with 10 or 12 l bottles. The CTD sampled at a rate of 33 Hz, and the data were filtered and averaged to 1 dbar bins. The conductivity measurements underwent quality control (and in some cases calibration) based on AUTOSAL estimates on bottle samples from the rosette. In some cases, to accommodate other sampling needs of the programs, multiple CTD casts (separated by a few hours) were used at each station. In these cases, the average profile was extracted and used for this study, so as to reduce possible noise in parameters like depth of isopycnals.

A Seabird Electronics SBE-13 dissolved oxygen sensor attached to the CTD provided continuous profiles of dissolved oxygen. The concentration of dissolved oxygen in water samples from distinct depths collected with the rosette sampler was measured by the Winkler method (Carpenter, 1965a, b). The discrete data obtained with the Winkler method were used to post-calibrate the continuous data of the SBE-13 sensor. These data underwent all the filtering and averaging applied to the CTD hydrographic measurements.

We selected one representative station from each of the distinct sub-basins of the North Aegean, i.e. Lemnos, Athos–North Sporades and North Skyros sub-basins, and produce mean profiles for each cruise in the region. The reason for selecting these depressions is simply data availability. Lemnos sub-basin is a 1550 m deep depression located nearest to the Dardanelles. North Skyros sub-basin is 980 m deep, and the maximum depth of Athos–North Sporades sub-basin is 1230 m—however, the depth at the region of our sampling at Athos station barely reached 900 m.

There have been no deployments of moorings dedicated to physical oceanography studies in the region under investigation. However, in the framework of the EU project MATER (Lykousis et al., 2002), a mooring directed to biogeochemical studies was deployed in each of the above-mentioned sub-basins of the North Aegean. The moorings were designed to monitor the downward flux of particulate material at intermediate depths (near 500 m) and near the bottom. Below each sediment trap there was an Aanderaa RCM-9

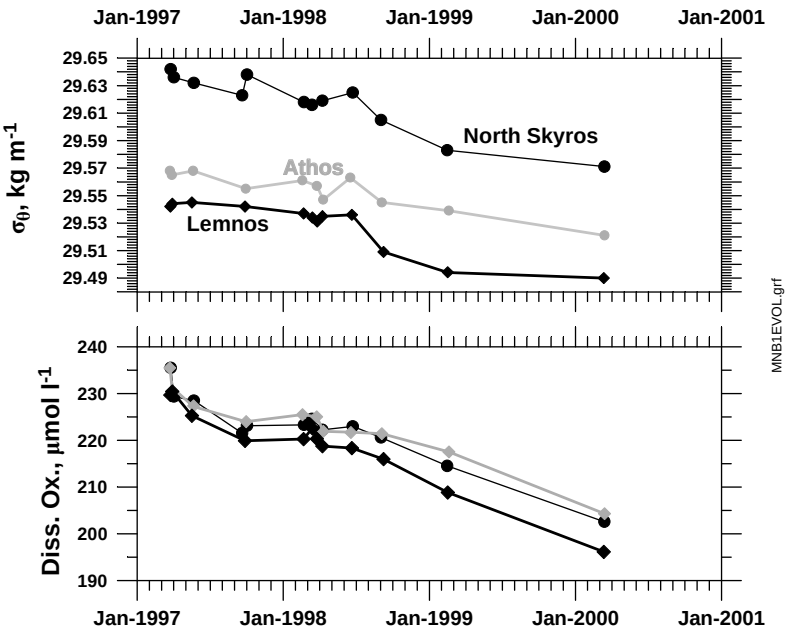

Fig. 4. The evolution of the mean vertically integrated density (top) and oxygen (bottom) at the three sub-basins of the North Aegean from March 1997 until March 2000. The limits of integration were 400–1000 m for the Lemnos basin (thick black line), 400–880 m for the Athos–North Sporades basin (gray line) and 400–750 m for the North Skyros basin.

current-meter sampling at hourly intervals, and right above the bottom there was another RCM-9. The RCM-9s were later recalled by the company in order to undergo improvements in the sensitivity of the acoustic sensor, an improvement that was judged necessary by Aanderaa for the operation in very clear waters, like the North Aegean. Despite that fact, the most of the velocity time-series collected with the current-meters passed our quality control tests. In Section 4 below we make a more extensive reference to the current velocity observations, and the data quality.

3. The estimation of eddy diffusivity K_c

3.1. Description of the model

The fact that bottom topography isolates the deeper-than-400 m layers of the various sub-basins of the North Aegean from each other and from the South Aegean during stagnation periods permits us to use a simple one-dimensional model to estimate vertical diffusion rates in each sub-basin. The model describes the balance between the time rate of change of the vertically integrated concentration of a passive tracer in the stagnant basin and the divergence of the vertical diffusive flux of tracer through the upper and lower boundaries of the volume considered. The above balance is more easily observed in lakes and reservoirs, as closed volumes can be easily determined and monitored, and the small volumes engaged result to large signal to noise ratios. Thus, the method has been used extensively in lakes (Jassby and Powell, 1975; Quay et al., 1980, Wüest et al., 1996) and fjords (Svensson, 1980; Smethie, 1980; Lewis and Perkin, 1982; Stigebrandt, 1976; Stigebrandt and Aure, 1989; Aure and Stigebrandt, 1989; Stigebrandt et al., 1996). More recently, Axell (1998) has used this method in estimating vertical diffusivities for deep sub-basins of the Baltic Sea during stagnation periods.

In oceanic environments such a method is not used extensively, because it is hard to determine closed basins where horizontal advection can be

neglected. Furthermore, most oceanic budget methods (Munk, 1966; Hogg et al., 1982; Whitehead and Worthington, 1982) assume an advective–diffusive balance rather than a temporal change—diffusive one. In this application, our observations suggest that the latter balance best describes the physics of our system during stagnation periods. The model we will use is similar to Axell's (1998), but we will re-derive the equations in order to identify some differences and assess possible sources of error.

Let c be the concentration of a conservative tracer. Then, its conservation is described by

$$\frac{\partial c}{\partial t}+\vec{u}_h\cdot\vec{\nabla}_h c+w\frac{\partial c}{\partial z}=\frac{\partial}{\partial z}\left(K_c\frac{\partial c}{\partial z}\right), \tag{1}$$

where the subscript h denotes horizontal component of a vector, and standard oceanographic notation has been used. The second term of the left-hand side expresses the changes due to divergence of advected c, and the third term represents quantities upwelled or transferred through convection processes. The right-hand side represents the change due to divergence of the turbulent flux of material, which is parameterized as a turbulent eddy diffusion term. K_c is the vertical eddy diffusivity; we assumed horizontal diffusion is incorporated in the horizontal advection term. The fact that there is no mean vertical motion during stagnation periods eliminates the upwelling/convection term. Horizontal integration throughout any whole horizontal surface at depths below 400 m in each sub-basin eliminates the horizontal advection terms, and Eq. (1) is reduced to

$$\frac{\partial}{\partial t}\int\int c\,\mathrm{d}x\,\mathrm{d}y=\frac{\partial}{\partial z}\left(\int\int K_c\frac{\partial c}{\partial z}\mathrm{d}x\,\mathrm{d}y\right). \tag{2}$$

Defining the horizontal mean $\langle c\rangle$ by $\langle c\rangle=(1/A(z))\iint c\,\mathrm{d}x\,\mathrm{d}y$, where $A(z)=\iint \mathrm{d}x\,\mathrm{d}y$, and assuming that $\langle K_c(\partial c/\partial z)\rangle\approx\langle K_c\rangle\langle\partial c/\partial z\rangle$, Eq. (2) can be rewritten as

$$A(z)\frac{\partial\langle c(z)\rangle}{\partial t}=\frac{\partial}{\partial z}\left(A(z)\langle K_c(z)\rangle\left\langle\frac{\partial c(z)}{\partial z}\right\rangle\right). \tag{3}$$

Henceforth, we will drop the symbols $\langle\rangle$ denoting horizontal averages, but the quantities c and K_c will be assumed horizontally averaged in each sub-basin. By vertically integrating Eq. (3) within the deep layer from the top of the considered layer z to the bottom D, we obtain

$$\bar{A}(z)\frac{\partial\bar{c}(z)}{\partial t}=\frac{1}{(z-D)}\times\left\{A(z)K_c(z)\left.\frac{\partial c}{\partial z}\right|_z-A(D)K_c(D)\left.\frac{\partial c}{\partial z}\right|_D\right\}, \tag{4}$$

where

$$\bar{c}(z)\equiv\frac{1}{(z-D)\bar{A}(z)}\int_D^z A(\zeta)c(\zeta)\,\mathrm{d}\zeta\quad\text{and}$$
$$\bar{A}(z)\equiv\frac{1}{(z-D)}\int_D^z A(\zeta)\,\mathrm{d}\zeta \tag{5}$$

are defined as the mean integrated values of c and A from z to D. The physical interpretation of (4) is that the change of the mean value of the property c within a layer of water equals the net input through the top and bottom of the layer.

3.2. Application of the model

Before actually applying the one-dimensional model described above to our case, we need to check if the change of hydrological characteristics of the sub-basins considered here is consistent with vertical mixing. For that purpose, we exploit the tool of θ/S diagrams. Fig. 5 is the concise history of the deep waters of each sub-basin presented as a θ/S diagram for each sub-basin. The continuous lines represent the θ/S properties at the beginning and at the end of the period 1997–2000. The symbols denote the 400 m and nearest-to-bottom data for each year of this period. The upper layers of the water column have been omitted for simplicity.

The first conclusion is that in general, the θ/S values lie along the same curve throughout the period. Furthermore, the inspection of the change of the hydrographic properties of the deeper-than-400 m layer over time reveals that the properties of the deep water "slide" along the θ/S curve, with a direction toward "lighter" water, i.e. towards the LIW water properties lying over the 400 m. This is a textbook example of vertical diffusive mixing, where the secluded, finite in volume water type of

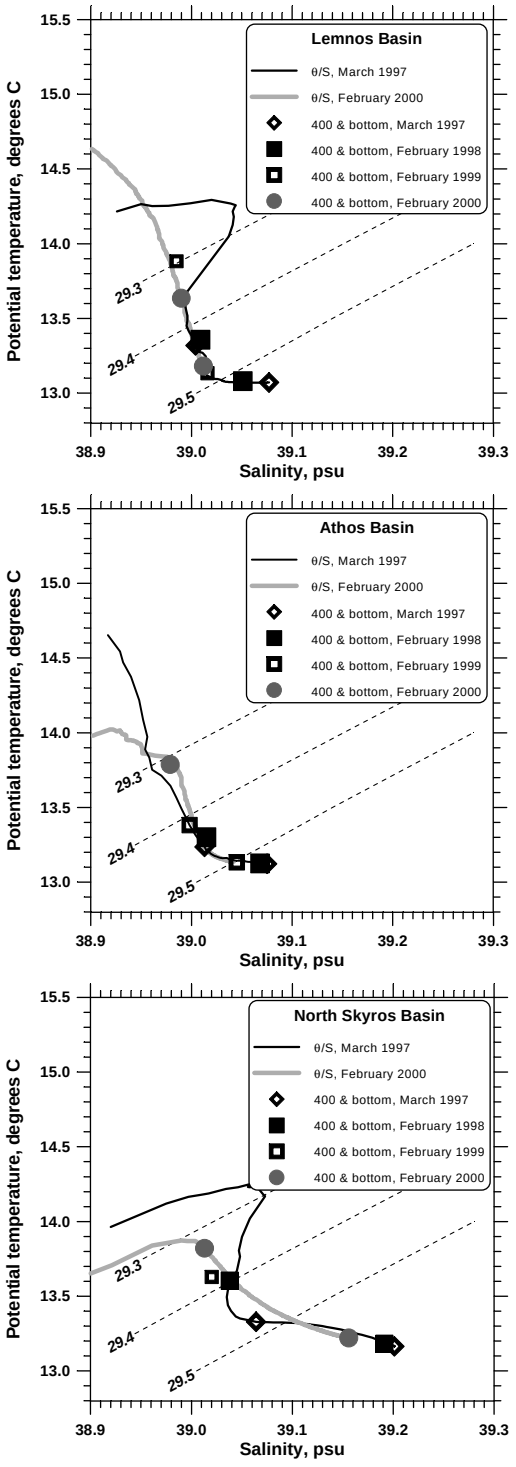

Fig. 5. The evolution of the deeper-than-400 m layer in the three sub-basins of Lemnos (top), Athos–North Sporades (middle) and North Skyros (bottom). The positions of the 400 m and the bottom measurement are shown by the same symbol, representative the time of sampling. Note that the points "drift" along the θ/S diagram toward smaller densities.

the bottom layer exchanges mass through mixing with the water passing over it. As the LIW waters coming from the South Aegean and Levantine represent a much larger water type and remain over the North Aegean sub-basins only for a finite time before being advected further by the general cyclonic motion of the Aegean, it is the deep waters that change their properties faster, "sliding" along the θ/S curve. Fig. 5 constitutes a solid justification that the simple one-dimensional model of vertical diffusion is valid for the deep layers of the North Aegean sub-basins during stagnation periods.

Through the various research cruises in the North Aegean we have collected hydrographic data that provide enough information of hydrographic parameters to estimate the left-hand side of (4), as well as the mean vertical gradients $\partial c/\partial z$ at the top and bottom of the considered layer. Thus, we are able to solve (4) for the eddy diffusion coefficient K_c:

$$K_c(z) = (z - D)\frac{\bar{A}(z)}{A(z)}\frac{\partial \bar{c}}{\partial t}\left(\frac{\partial c}{\partial z}\Big|_z\right)^{-1} + K_c(D)\frac{A(D)}{A(z)}\frac{\partial c}{\partial z}\Big|_D\left(\frac{\partial c}{\partial z}\Big|_z\right)^{-1}. \quad (6)$$

The only unknown parameter of the right-hand side is the value of the eddy diffusion coefficient $K_c(D)$ at the bottom of the layer of integration. Most investigators (Stigebrandt, 1976; Stigebrandt and Aure, 1989; Stigebrandt et al., 1996; Axell, 1998) in the past have ignored the last term of the right-hand side, assuming that the flux at the bottom of the basin is zero. If the bottom boundary of the layer considered is indeed the bottom of the basin, the assumption is well founded and one needs to consider only the flux at the top of the layer. However, when the bottom of the considered layer is not the bottom of the basin, one cannot ignore the flux through the

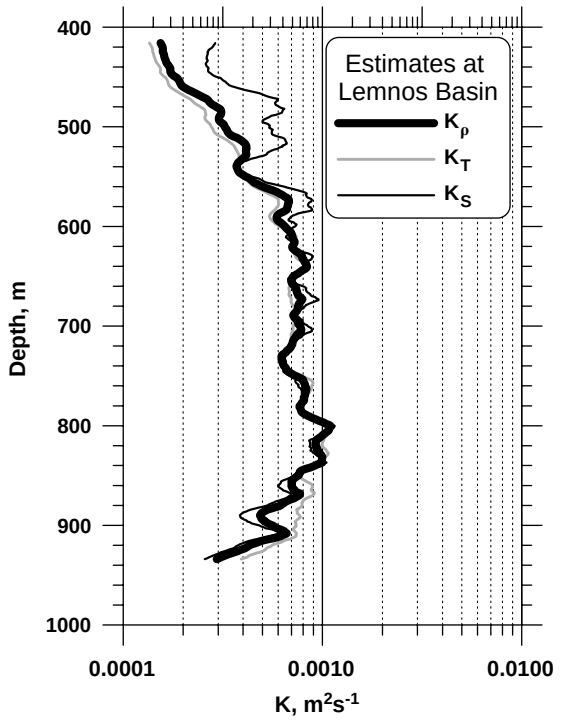

Fig. 6. Estimates of vertical eddy diffusivity based on salinity (K_S, thick black line), temperature (K_T, gray line) and density (K_ρ, thin black line). A bottom value of $K(D) = 10^{-4}\,m^2\,s^{-1}$ at the layer bottom at $D = 950\,m$ was used for all estimates.

bottom of the layer. Thus a vertical eddy diffusion coefficient $K_c(D)$ has to be provided at $z = D$.

Sensitivity to tracer. The sensitivity of the method to the selection of different tracers is tested by calculating vertical diffusivities using temperature, salinity and density as tracer (Fig. 6). In the case of temperature and density, we utilized the potential quantities, in order to account for the compression effect. For the estimates presented in Fig. 6, we provided a hypothetical $K_S(D) = K_T(D) = K_\rho(D) = 10^{-4}\,m^2\,s^{-1}$ at the bottom of the layer under consideration. The agreement of all three eddy coefficients is striking in the deeper than 500 m layers, and within a factor of 2 between 400 and 500 m. The good agreement of the three diffusivity estimates suggests that the dominant process in vertical diffusion was turbulent mixing, and permits us to use only one of the three parameters in order to estimate vertical diffusion coefficients. Hereafter, we will make estimates of K_ρ only, as the other diffusivities are expected to be the same assuming active turbulent mixing in each basin.

Sensitivity to bottom diffusivity $K_\rho(D)$. As mentioned above, the uncertainty of $K_\rho(D)$ turns the second term of the right-hand side of Eq. (5) into a potential source of error for the estimation of $K_\rho(z)$. The assessment of this potential error is important in this work—and is the major difference with previous works—as often our CTD casts did not reach the bottom of the basins. In order to explore the range of error introduced to the $K_\rho(z)$ estimate by the inclusion of the $K_\rho(D)$ term, we proceeded to produce $K_\rho(z)$ estimates using $K_\rho(D)$ values of 10^{-5}, 10^{-4} and $10^{-3}\,m^2\,s^{-1}$ (Fig. 7). Note that the various estimates agree very well with each other away from the lower integration limit, and that only within the bottom 150 m of the

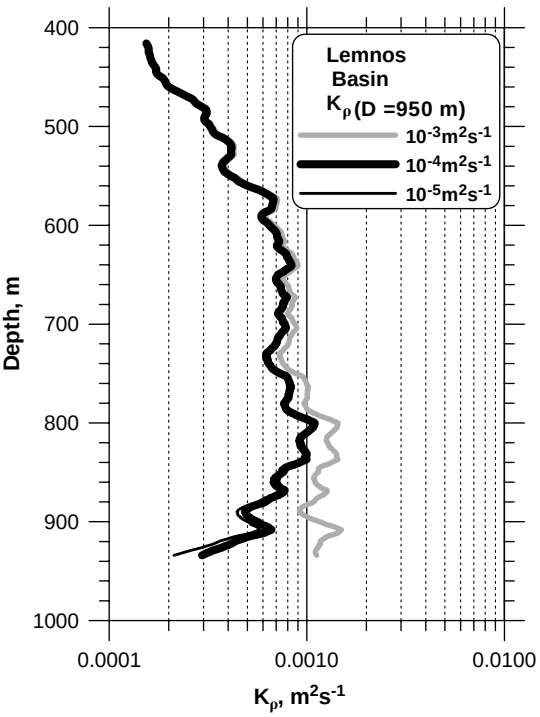

Fig. 7. Sensitivity of the $K_\rho(z)$ estimate on the selection of $K_\rho(D)$, for Lemnos Basin. The estimates for $K_\rho(D) = 10^{-5}\,m^2\,s^{-1}$ (thin black line), $10^{-4}\,m^2\,s^{-1}$ (thick black line) and $10^{-3}\,m^2\,s^{-1}$ (gray line) are presented.

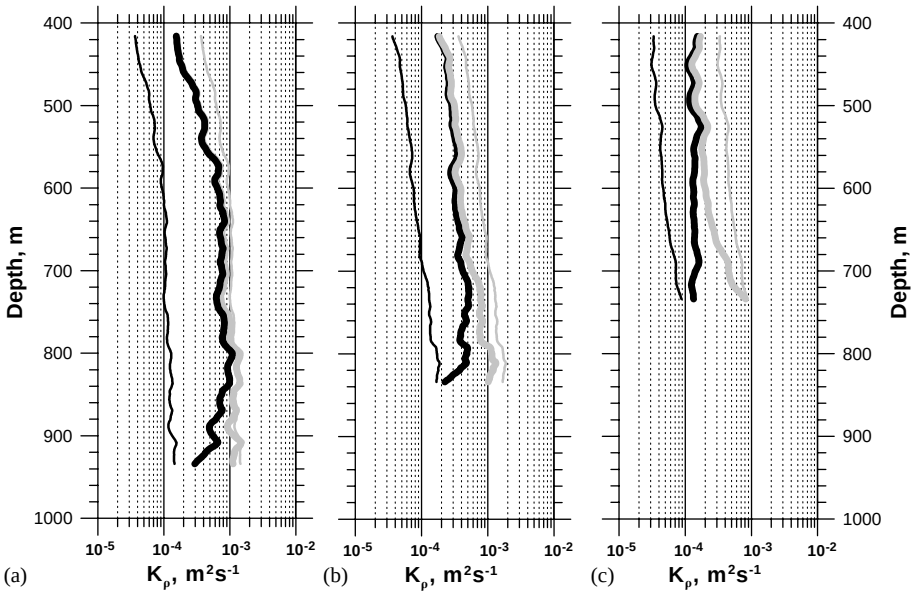

Fig. 8. The $K_\rho(z)$ estimates for (a) Lemnos basin, (b) Athos–North Sporades basin and (c) North Skyros basin. The thick black lines represent estimates made for $K_\rho(D) = 10^{-4}\,m^2\,s^{-1}$, thick gray lines for $K_\rho(D) = 10^{-3}\,m^2\,s^{-1}$. The thin lines represent parameterized $K_\rho(z) = \alpha\, N^{-1}$ estimates, with $\alpha = 1 \times 10^{-7}\,m^2$ (thin black line) and $\alpha = 10 \times 10^{-7}\,m^2$ (thin gray line).

integration is there a significant deviation of the $K_\rho(D) = 10^{-3}\,m^2\,s^{-1}$ estimate.

Eddy diffusivity in the three basins. In all subbasins, the eddy diffusivity at about 400 m is in the order of $1–2 \times 10^{-4}\,m^2\,s^{-1}$ (Fig. 8). This value increases rapidly with depth in Lemnos basin, to reach to about $8 \times 10^{-4}\,m^2\,s^{-1}$ at 600 m, and $10 \times 10^{-4}\,m^2\,s^{-1}$ at 800 m depth. Below that depth, the eddy diffusion coefficient estimate depends largely on its assumed value at 950 m. Contrary to the Lemnos basin K_ρ profile, the diffusivity rises only to $4–5 \times 10^{-4}\,m^2\,s^{-1}$ in Athos–North Sporades basin, and remains at $1–2 \times 10^{-4}\,m^2\,s^{-1}$ at North Skyros basin (not considering the results below 700 and 600 m, respectively, because of dependence on the assumed value of K_ρ at the bottom of the considered layer).

In order to assess these estimates we compare with Gargett and Holloway (1984) and Gargett's (1984) parameterization for eddy diffusion coefficient in the deep ocean based on internal wave theory and statistics:

$$K_\rho = aN^q, \tag{7}$$

where $N(z)$, the buoyancy frequency at depth z, is defined by $N^2 \equiv -(g/\rho)\mathrm{d}\rho/\mathrm{d}z$. We use Eq. (7) to assess the adequateness of the Gargett (1984) parameterization in the relatively tideless deep basins of the North Aegean, despite the fact that it is derived (and expected to hold) in the open ocean, away from boundary mixing. In (7) we used $q = -1$, as suggested by Gargett (1984). For the coefficient α we used two values: the oceanic value of $1 \times 10^{-7}\,m^2$ as suggested by Gargett (1984), and a value of $10 \times 10^{-7}\,m^2$, one order of magnitude larger. Fig. 8 reveals that in Lemnos basin, the coefficient $\alpha = 10 \times 10^{-7}\,m^2$ describes better the vertical diffusion processes; in the other two basins the best fits would be produced with $\alpha \approx 4–5 \times 10^{-7}\,m^2$. In all cases, the parameterization required for a best fit to the K_ρ estimates is much larger than Gargett's α coefficient for the open ocean. We note that the selection of diffusivity at the bottom of the considered layer determines to a large degree how close our estimate will be to parameterization (7). A selection of small diffusivity, of the order of 10^{-4}, results in significant deviations at depth between

the observed profile of K_ρ and the profiles according to Gargett (1984).

4. Comparison to internal wave energy levels

The first suspect responsible for different mixing rates in each sub-basin would be differences in the energetics of the internal wave field. In order to assess the internal waves, velocity spectra were computed on 1024-point long segments of the current-meter records, and then the method of rotary decomposition (Gonella, 1972) was employed to separate the clockwise from the counter-clockwise rotating parts of the velocity. Furthermore, in order to compare with the expected open-ocean internal wave field, we estimated the corresponding Garrett–Munk spectrum (Garrett and Munk, 1979) as presented by Munk (1981) using local values of buoyancy frequency obtained from hydrographic cruises in the region. The rotary spectra and the corresponding Garrett–Munk levels for each sub-basin are presented in Fig. 9.

We note that away from the bottom, the G–M model very well approximates the internal wave field: the slope of the spectrum is –2 at high frequencies, and the energy levels are within an order of magnitude of the G–M prediction. Of interest is the fact that the IW field appears to be more energetic than in the open ocean, despite the fact that a significant source of internal waves, the tides, is essentially non-existent in this semi-enclosed sea.

The nearest-to-the-seabed (about 10 m off the bottom) current-meters exhibit an unexpected behavior, as the spectrum is white at high frequencies: whereas the energy levels at very low frequencies, close to the inertial, are at expected levels, the spectra soon turn "red", the slope

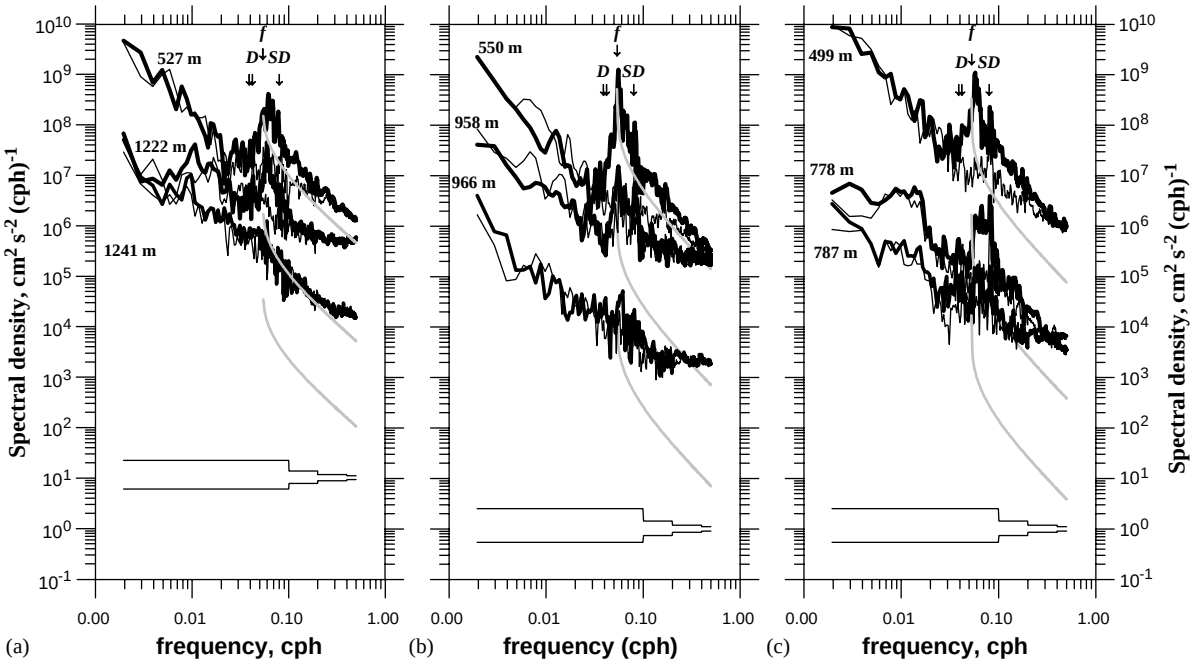

Fig. 9. Rotary spectra of velocity from (a) Lemnos basin, (b) Athos–North Sporades basin and (c) North Skyros basin. Both the clockwise (heavy line) and counter-clockwise (light line) spectra of the current are presented. The bottom current-meter spectra are presented without offset; the deep and upper current-meters are presented with an offset of 2 and 4 orders of magnitude respectively. For comparison, the Garret–Munk spectra estimated for each depth are presented (gray lines), with the same offset as above. The G–M spectra are plotted not all the way to the local buoyancy frequency, but until the Nyquist frequency of the data. The 95% confidence intervals are presented at the bottom, and the positions of the inertial (f), semidiurnal (SD) and diurnal (D) peaks are identified.

approaches zero and the energy near the Nyquist frequency becomes higher than the G–M expectation by 2–3 orders of magnitude. In the Lemnos and Athos–North Sporades sub-basins, the high-frequency energy enhancement is recorded not just by the bottom current-meters but by the current-meters positioned about 10 m above them as well. The local N (Brunt-Väisälä) frequency is about 0.5 cph near the bottom and 1 cph at 500 m. Based on earlier studies of internal wave reflection on sloping bottoms, we would expect an increase of the IW energy near the critical frequency, which is a function of bottom slope, buoyancy frequency and local Coriolis frequency. The moorings were deployed near the bottom of the sub-basins, and the large-scale slope of the seabed should be zero, while the small-scale slope, based on bathymetric maps, does not exceed 0.25. As there has not been a high-resolution bathymetric survey around the moorings, we are not able to provide an exact estimate of the local critical frequency. Based on the estimates from bathymetric maps, we would expect that the critical frequency should be at the neighborhood of the local inertial frequency (Phillips, 1977; Garrett and Gilbert, 1988; Eriksen, 1982, 1985, 1998a, b), but an effect of internal wave energy enhancement at a low critical frequency is not apparent in Fig. 9.

5. The role of bottom topography

In the effort to explain the differences in the estimated eddy diffusivities between the sub-basins, we should consider the shape of the seabed in each case. According to Gilbert and Garrett (1989), convex topography should induce energy enhancement near the critical frequency of the internal waves, in contrast to concave topography, which should cause no such an enhancement. In order to generate a representative shape of the seabed for each sub-basin, we assumed a circular cross-section and based on the area of the sub-basin at each depth we estimated the radius of the circular basin (Fig. 10). In order to classify basins as concave or convex, we have used the concavity criterion proposed by Gilbert (1993), which is equivalent to examining concavity in a WKB-stretched vertical coordinate space (Gilbert, 1990). It is noteworthy that the vertical profile of the seabed in Lemnos basin is near critical below 600 m, and clearly convex in the vicinity of 800 m;

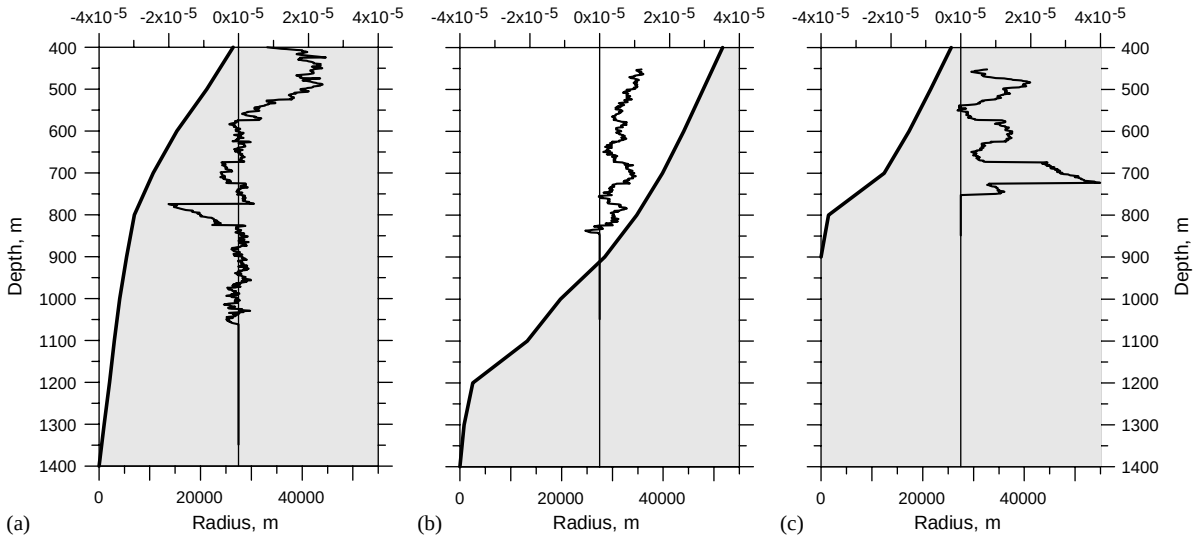

Fig. 10. Representative bottom topography of (a) Lemnos, (b) Athos–North Sporades and (c) N. Skyros basin. The profiles were estimated by assuming a circular cross-section, and estimating the radius from the area of the basin at each depth. Overlaid are graphs of the concavity criterion (top axis) as a function of depth. Positive values suggest concave shape, negative value convex.

Table 1

	Lemnos basin	Athos–N. Sporades basin	North Skyros basin
P (500 m) ($\times 10^{-2}$ W m^{-2})	0.1282	0.0935	0.0938
Δh below 500 m (m)	148	316	146
ε ($\times 10^{-6}$ W m^{-3})	8.662	2.959	6.424

the seabed at the other two basins is concave (Fig. 10). The fact that much higher diffusivity characterizes the former basin than the latter two is in good agreement with Gilbert and Garrett's (1989) prediction that convex topography induces energy enhancement near the critical frequency of the internal waves, in contrast to concave topography, which causes no such enhancement. Thus, as a result of the energy enhancement at the critical frequency, we expect the development of internal wave breaking and higher dissipation rates. Indeed, internal wave measurements over locally convex topography suggest enhancement of energy near the critical frequency (Thorpe, 1987; Wunsch and Hendry, 1972). However, we have to ensure that the higher eddy diffusivity estimated at Lemnos basin is indeed attributed to enhanced mixing due to the convex shape of the basin and not an artifact of convex basins simply having less water than concave ones. In order to test this possibility we estimated the internal wave energy flux $P(z)$ (following Axell, 1989) through the isobath at depth z for each basin.

$$P(z) = \frac{g}{R_f A(z)} \int_H^z \frac{\langle \mathrm{d}\rho(\zeta) \rangle}{\mathrm{d}t} (\zeta - z) A(\zeta)\, \mathrm{d}\zeta, \qquad (8)$$

where R_f the flux Richardson number (~ 0.1), g the acceleration of gravity and $\langle \rho(\zeta) \rangle$ the horizontally averaged density at depth ζ. The estimated fluxes, divided by the mean depth of each basin *below* the 500 m isobath provides the mean dissipation plus work against buoyancy forces at each basin. The results are presented in Table 1 below.

The energy flux is about the same both at Athos–N. Sporades and North Skyros basins, however this energy is distributed over a layer 316 m on average in the former basin and 146 m in the latter basin. As a result, there is more significant mixing in the North Skyros basin due to its smaller volume of water. This increased mixing is not reflected in the K_ρ values, as the size of the basin has been taken into account in the K_ρ estimation (Eq. (6)).

The energy flux at Lemnos basin is about 27% higher than the other two basins. While the mean thickness of the layer below 500 m at Lemnos is similar to North Skyros basin, the average dissipation in the former is estimated to be 25% higher than the latter, a difference that is attributed to different dynamics of mixing in the two basins.

We were unable to directly measure enhancement of the internal wave energy, because the moorings were positioned not over the slope but over the bottom of the basins. However, this work presents indirect evidence that increased mixing may result in basins characterized by convex topography, possibly by enhanced breaking of internal waves.

6. Estimating oxidation rates

It is common practice in oceanographic literature to assess the organic matter oxidation rates by estimating the rate of change of dissolved oxygen concentration (henceforth: c_{DO}) and assume that the c_{DO} decay is attributed entirely to the oxidation of organic matter (Souvermezoglou and Krasakopoulou, 2002). The estimation of vertical eddy diffusivity performed above allows an improvement of the estimates of deep-water organic matter oxidation rates based on the rate of change of c_{DO}. The dissolved oxygen concentration in each layer of the deep sub-basins during stagnation periods will depend on the divergence of turbulent diffusive flux of dissolved

oxygen through the layer and the local consumption by organic matter oxidation. The following equation (analogous to Eq. (2)) expressing this budget is

$$\frac{\partial}{\partial t}\iint c_{DO}\,dx\,dy = \frac{\partial}{\partial z}\left(\iint K_\rho \frac{\partial c_{DO}}{\partial z}\,dx\,dy\right) - \iint Q\,dx\,dy, \quad (9)$$

where Q is the consumption of dissolved oxygen by oxidation of organic matter. Using the same notation conventions as above and following a similar procedure of vertical averaging for a layer between the depths D_1 and D_2, we obtain

$$\bar{A}\frac{\partial \bar{c}_{DO}}{\partial t} = \frac{1}{(D_1 - D_2)}\left\{A(D_1)K_\rho(D_1)\left.\frac{\partial c_{DO}}{\partial z}\right|_{D_1} - A(D_2)K_\rho(D_2)\left.\frac{\partial c_{DO}}{\partial z}\right|_{D_2}\right\} - \bar{A}\bar{Q}, \quad (10)$$

which can be solved for $\bar{Q}$:

$$\bar{Q} = -\frac{\partial \bar{c}_{DO}}{\partial t} + \frac{1}{(D_1 - D_2)}\left\{\frac{A(D_1)}{\bar{A}}K_\rho(D_1)\left.\frac{\partial c_{DO}}{\partial z}\right|_{D_1} - \frac{A(D_2)}{\bar{A}}K_\rho(D_2)\left.\frac{\partial c_{DO}}{\partial z}\right|_{D_2}\right\}. \quad (11)$$

Eq. (11) is solved with the K_ρ profiles for each sub-basin estimated in the previous sections. We estimate the mean integrated Q over layers of 50 m thickness. The lower 150 m of each K_ρ profile estimated in the previous sections are discarded, so as to ensure that the uncertainty due to the unknown flux through the bottom boundary is not introduced in this analysis. The results are presented in Fig. 11.

In Lemnos basin, the estimated Q is about 11.2 μmol l^{-1} yr^{-1} in the layers between 460 and 620 m, increasing to about 13.4 μmol l^{-1} yr^{-1} from 620 to 760 m. In contrast, the consumption of dissolved oxygen in Athos–North Sporades basin decreases with depth, from 10.2 μmol l^{-1} yr^{-1} in the layer 460–510 m to 4.9 μmol l^{-1} yr^{-1} in the

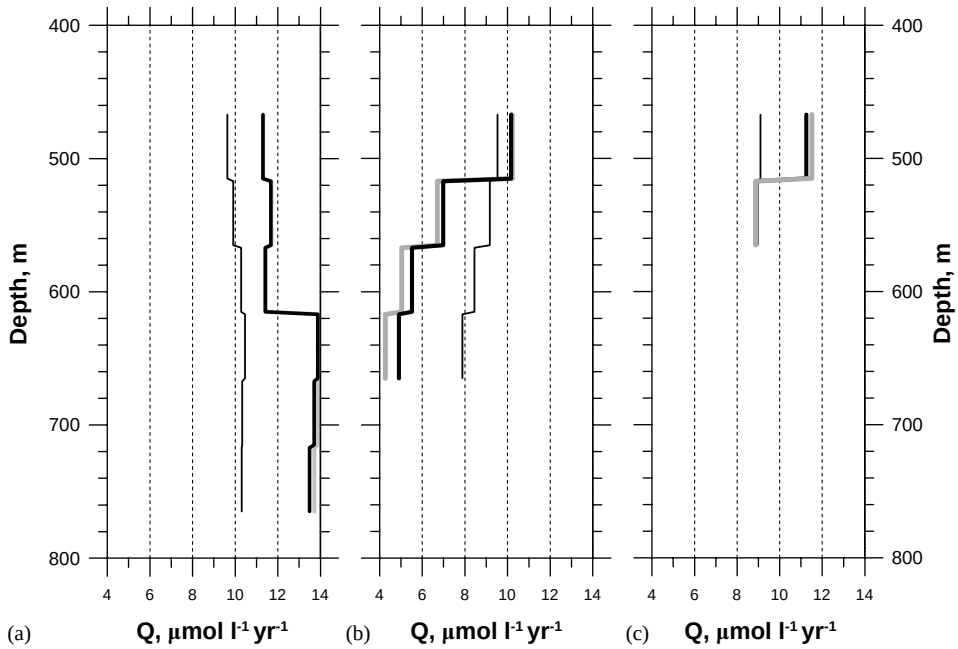

Fig. 11. Estimates of the consumption of dissolved oxygen based on $K_\rho(D) = 10^{-4}\,m^2\,s^{-1}$ (thick black line) and on $K_\rho(D) = 1\times10^{-3}\,m^2\,s^{-1}$ (thick gray line) for (a) Lemnos, (b) Athos–North Sporades and (c) North Skyros basins. The thin black line displays the estimated rate of decay of c_{DO}.

layer 620–660 m. In North Skyros basin, the consumption is $11.2\,\mu mol\,l^{-1}\,yr^{-1}$ in the layer 460–510 m and $8.9\,\mu mol\,l^{-1}\,yr^{-1}$ from 510 to 560 m. In all basins, the estimates of Q where essentially independent of the choice of $K_\rho(D)$.

The comparison between our estimates of Q and the measured rate of decay of dissolved oxygen concentration, $\partial c_{DO}/\partial t$, showed that in Lemnos basin $Q > \partial c_{DO}/\partial t$, but in the deep layer of Athos–North Sporades basin $Q < \partial c_{DO}/\partial t$. In the upper layer of North Skyros basin $Q > \partial c_{DO}/\partial t$, but in the deeper layer $Q \cong \partial c_{DO}/\partial t$. In order to interpret these results, we have to consider the vertical profiles of dissolved oxygen concentration and their evolution in time (Fig. 12).

For the time period considered here, the oxycline $\partial c_{DO}/\partial z$ remains positive (assuming z increasing upwards) in both Lemnos and North Skyros basins. As a result, the vertical flux of dissolved oxygen due to turbulent mixing processes will be downwards. The divergence of this flux is the oxygen gained and available for consumption in each of the considered layers. In the previous sections we have shown that mixing is significantly higher in Lemnos basin than in both the other basins, and thus the oxygenation in the deep layers of Lemnos basin is much stronger than in the other two basins. At the same time dissolved organic matter (DOM) that accumulates in the upper layers is pumped with higher intensity into the deep waters of Lemnos basin. In some early studies vertical eddy diffusion is referred to as the main physical mechanism injecting semi-labile DOC (with a residence time of months) into deep waters under stratified conditions (Copin-Montegut and Avril, 1993; Carlson et al., 1994; Doval et al., 2001). The DOM exported downwards by turbulent diffusion together with the particulate organic matter (POM) produced in and settling from the euphotic zone are remineralized, contributing to the observed decay rate of dissolved oxygen (Q). As a consequence, the estimates of Q in Lemnos basin are 20–30% higher than the observed rate of decay of dissolved oxygen, while in North Skyros basin the calculated oxygen consumption exceeds by 0–25% the recorded values.

In contrast to the other two basins, the slope of the oxycline in Athos–North Sporades basin, which is zero or slightly positive in 1997, becomes negative after 1999 (Fig. 12). As there has been no

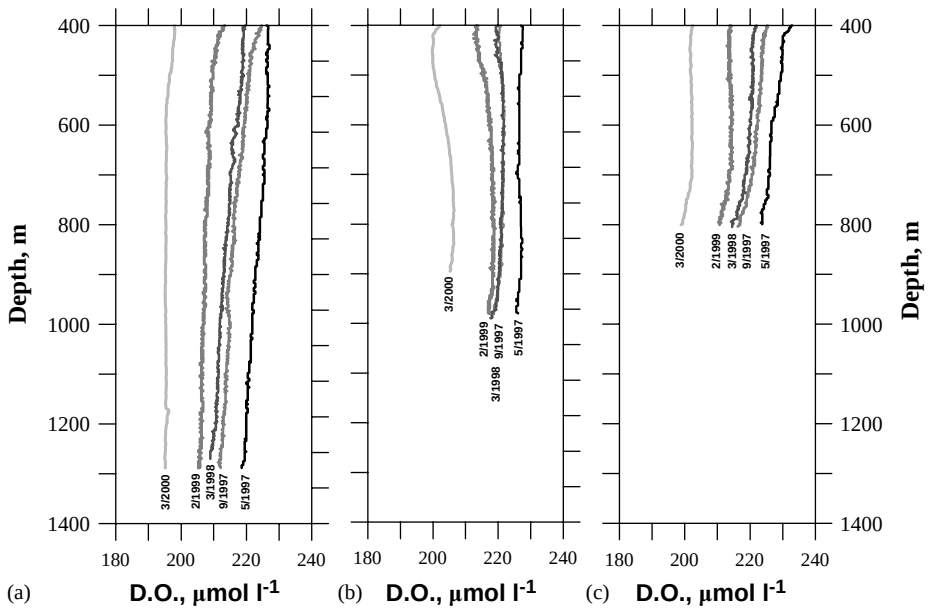

Fig. 12. Vertical profiles of c_{DO} for the various cruises as recorded in (a) Lemnos, (b) Athos–North Sporades and (c) North Skyros basins.

near-bottom water formation event in the period considered, the development of a negative oxycline in the absence of horizontal advection can be attributed only to a differential consumption of dissolved oxygen between the upper and lower parts of the deep layer of Athos sub-basin. Indeed, our estimate of Q suggests that while Q is comparable to $\partial c_{DO}/\partial t$ in the 460–510 m layer of the sub-basin, it falls rapidly with depth to a level much smaller than $\partial c_{DO}/\partial t$ near the bottom. Furthermore, the estimate of oxygen consumption in the deepest parts of Athos–North Sporades basin is much smaller than the corresponding estimates for the other two basins. This result is also certified by the fact that the measured value of dissolved oxygen concentration near the bottom of Athos–North Sporades basin (205.3 $\mu mol\,l^{-1}$) is higher than the values recorded in the other two basins (196.4–200.9 $\mu mol\,l^{-1}$). The negative slope of Athos–North Sporades basin turns the diffusive flux of dissolved oxygen upwards. The deep layers become a source of dissolved oxygen for the intermediate ones, and less oxygen is available for consumption.

Based on the above estimates of consumption of dissolved oxygen for the oxidation of organic matter, we can quantify the intensity of the carbon pump in the region of the North Aegean Sea. Assuming that the oxygen decay due to organic matter remineralization in the deep layer of each sub-basin remains stable down to the bottom boundary, the total integrated rates of oxygen consumption for the deeper than 460 m layer for the three depressions expressed as mmol $O_2\,m^{-2}\,d^{-1}$ are estimated as 27.8 (Lemnos), 8.7 (North Skyros) and 7.4 (Athos–North Sporades). The carbon flux needed to support the oxygen consumption can be determined by converting oxygen to carbon equivalents according to the Redfield stoichiometry ($-O_2$:C=1.3). The results are 21.4, 6.7 and 5.7 mmol $C\,m^{-2}\,d^{-1}$, respectively, for the three depressions.

7. Discussion

The vertical eddy diffusivities estimated from the simple one-dimensional model used here are significantly higher than values estimated with either similar models (Axell, 1998) or advection–diffusion balance models (Munk, 1966; Hogg et al., 1982) in the open ocean, and in general they are much higher than direct measurements of dissipation in the open ocean (Gregg, 1998). Furthermore, the eddy diffusivities do not vary proportionally to the internal wave energy levels observed in each sub-basin. Clearly, the main contributor to vertical turbulent mixing is not the internal wave field away from the boundary, but rather near the seabed. Considering that most of the breaking of the internal wave field is expected to take place over the continental slopes, the large values of K_ρ should be expected, considering the small size of the North Aegean sub-basins. The current eddy diffusivity estimates correspond to sub-basin average profiles, and the local values within a hundred meters of the slope could be much higher than away from it, as many authors suggest, based on theoretical studies as well as measurements of internal wave characteristics over the continental slope. Several recent observations have revealed the role of topography in removing energy from the internal wave band (and mostly baroclinic tides) to turbulent mixing and dissipation (Lueck and Mudge, 1997; Kunze and Toole, 1997; Toole et al., 1997; Garrett, 2000; Lien and Gregg, 2001). Using deep dissipation measurements, Toole et al. (1997) have estimated eddy diffusivities exceeding $2\times10^{-3}\,m^2\,s^{-1}$ over the continental slope of the east coast of Brazil Basin, which fall to background levels of the order of $10^{-5}\,m^2\,s^{-1}$ over the open ocean. Ledwell and Hickey (1995) and Ledwell and Bradkovich (1995), through a tracer release experiment in the ocean, provided further evidence for enhanced mixing near the slope, resulting to an average diffusivity estimate higher than the values measured away from the boundaries. Our estimated diffusivities fall well within the expected values, considering they are horizontal averages and the small size of the sub-basins. Furthermore, our estimates are consistent with Gilbert and Garrett's (1989) prediction that enhanced internal-wave-induced mixing should take place over convex compared to concave topography.

The difference in the intensity of mixing between the three sub-basins has its effect on the decay rate of c_{DO} in each basin. In a comprehensive analysis of the evolution of dissolved oxygen concentration in the deep North Aegean during the 1980s and 1990s, Souvermezoglou and Krasakopoulou (2002) have shown that after a deep water formation event the rate of decay of c_{DO} in the deep layers is very high initially, and it decreases after several years. Consideration of the vertical diffusive flux of oxygen can provide some explanation for such a finding: Assuming the majority of the new dense water is formed over the shelf, then immediately after a formation event, the deep layers in the North Aegean have higher concentration of dissolved oxygen than the aged Levantine Intermediate Water above them. Thus, the oxycline will be negative, the diffusive flux of oxygen will be upwards and the measured rate of decay of oxygen will be higher than the local oxidation rate. In contrast, long after a formation event, when the deep layers have less oxygen than the intermediate, the diffusive flux of oxygen will be downwards and the rate of decay of oxygen will be less than the local oxidation rate. In addition, it must be mentioned that just after the dense water formation event the deep layers are fuelled with large quantities of "fresh" dissolved and particulate organic matter that undergoes bacterial consumption supporting thus elevated oxygen utilization rates. Progressively the contribution of this organic matter to the local oxidation rates becomes less significant as its easily oxidizable fraction is exhausted and the residual becomes more and more recalcitrant. Finally, long after a formation event, the consumption of dissolved oxygen by oxidation of organic matter is mainly controlled by the oxidation of the organic particles falling from the upper parts of the water column and the DOM exported downwards by turbulent diffusion.

Primary productivity in the euphotic zone is the process that initiates the transport of organic carbon from the surface to the deep ocean. A large fraction of the primary production is recycled within the photic layer, whereas the remainder escapes to the aphotic layer. It is also considered that the particulate organic carbon recycled in the photic layer or degraded and exported in dissolved form could amount to 85–95% of the primary productivity (Eppley and Peterson, 1979; Martin et al., 1987; Miquel et al., 1994; Durrieu de Madron et al., 2000). Considering that the average annual primary production measured in 1997 in the same area was estimated to be about $70\,\mathrm{mmol\,C\,m^{-2}\,d^{-1}}$ (Siokou-Frangou et al., 2002), the POC removed from the upper layer and transported downwards is $\sim 7\,\mathrm{mmol\,C\,m^{-2}\,d^{-1}}$. Interestingly this amount of carbon is slightly higher than the required quantity to sustain the calculated Q in N. Skyros and Athos–North Sporades basins. In contrast to the former, in Lemnos basin this amount represents only one third of the carbon demand, suggesting either that the settling particles are not the major source of carbon in the deep layer of the basin and that a significant amount of dissolved organic carbon is exported from the upper waters by the diffusive process, and/or that particulate organic carbon export is more efficient than in the other basins. We suggest that the former is true, as the basin-integrated diffusive flux of dissolved organic carbon would not vary much throughout the water column due to the shape of the seabed.

The rates of oxygen consumption (Q) estimated in the North Aegean deep basins are significantly higher than the oxygen utilization rates based on open ocean composite C fluxes ($1.07\,\mu\mathrm{mol\,O_2\,l^{-1}\,yr^{-1}}$ at 500 m depth; $0.29\,\mu\mathrm{mol\,O_2\,l^{-1}\,yr^{-1}}$ at 1000 m depth; Martin et al., 1987). They are also one order of magnitude higher than the oxygen consumption rate determined by fitting simulated oxygen concentrations obtained by a box model to observations from a medium resolution survey of the Eastern Mediterranean ($0.53\,\mu\mathrm{mol\,O_2\,kg^{-1}\,yr^{-1}}$ depth $\geqslant 1000$ m; Roether and Well, 2001). However, the oxygen consumption rates in Athos–North Sporades and North Skyros sub-basins are found to be rather close to the oxygen utilization rate of $4.4\,\mathrm{mmol\,O_2\,m^{-2}\,d^{-1}}$ estimated from electron transport activity (ETS) measurements in the depth range of 200–1000 m of the northwestern Mediterranean Sea (Lefevre et al., 1996).

These sub-basins in the North Aegean constitute ideal experimental sites for studying the effect of topography on internal wave energy enhancement near the local critical frequencies, and the resulting mixing. Furthermore, because of the small size of the sub-basins and the relative scarcity of deep-water formation events, it is possible to use simple one-dimensional models to estimate vertical diffusivity and compare with locally measured values through deep microstructure measurements. The potential cost of a dedicated experiment would be much reduced compared to an oceanic experiment by the small distances between the various sub-basins, as well as of the sub-basins to the coast. The fact that the region of the North Aegean Sea could be a region where events like the Eastern Mediterranean Transient may be triggered (Zervakis et al., 2000), as well as the role of the Dardanelles outflow in enhancing the productivity of the oligotrophic Aegean, only add to the oceanographic interest in this region.

8. Conclusions

In this work, we exploit hydrographic data collected in the deep sub-basins of the North Aegean during long periods of stagnation in order to estimate the intensity of mixing in each sub-basin.

The use of θ/S diagrams has certified that a one-dimensional model would be adequate for our purposes, as the evolution of the hydrographic properties was compatible with vertical mixing.

The model used required the parameterization of the near-seabed eddy diffusivity, and our results showed some sensitivity to that parameter. However, higher than 150 m from the deepest measurement, our diffusivity estimates were rather insensitive to the buoyancy diffusive flux near the bottom, most probably due to the low stratification there. Our results suggest that the most intense mixing takes place in the deep Lemnos basin, reaching a maximum of $K_\rho \cong 10^{-3}\,\mathrm{m^2\,s^{-1}}$, and the weakest in Athos–North Sporades basin, of the order of $K_\rho \cong 10^{-4}\,\mathrm{m^2\,s^{-1}}$. These values are still considered very high for open ocean standards, and should probably be attributed to the proximity to the continental slope. Furthermore, the intense mixing in Lemnos basin may be due to its convex topography, which could be inducing internal wave energy enhancement near the critical frequency and mixing.

Exploitation of the diffusivity estimates along with a time-series of dissolved oxygen profiles allowed the estimation of organic matter oxidation rates in the deep sub-basins and comparison to the observed rate of decay of dissolved oxygen. Lemnos basin constitutes a much more effective pump of carbon, with an oxidation rate reaching $13.4\,\mu\mathrm{mol\,l^{-1}\,yr^{-1}}$, while the Athos–North Sporades basin exhibited very small oxidation rates at depths greater than 600 m, barely exceeding $4.9\,\mu\mathrm{mol\,l^{-1}\,yr^{-1}}$. Furthermore, we have shown that the slope of the oxycline can be critical in determining the oxidation rate in the deep waters.

Comparison of the estimates of organic carbon demand that would sustain the calculated through the model oxygen consumption rates with primary production estimates suggests that the dissolved fraction of organic carbon is relatively more important for the carbon supply in the deep layers of Lemnos basin than in N. Skyros and Athos–North Sporades basins.

Acknowledgements

This work was supported partly by the European Commission DG-XII, Marine Science and Technology MTP-II MATER project, contract no. PL950401, and partly by the Ministry of National Finances, through the project "Infrastructure development for the study of pollutants entering the N. Aegean Sea via rivers and the Black Sea". We are indebted to Chris Garrett for his valuable comments and encouragement. Also, we thank Adolf Stips and Murray Levine, as well as three anonymous reviewers for helping to significantly improve the manuscript through their comments. We wish to thank the captain, officers and crew of the R/V *AEGAEO* for the generous offer of their expertise throughout several campaigns in the Aegean Sea.

References

Axell, L.B., 1998. On the variability of Baltic Sea deepwater mixing. Journal of Geophysical Research 103 (C10), 21667–21682.

Aure, J., Stigebrandt, A., 1989. On the influence of topographic factors upon the oxygen consumption rate in sill basins of Fjords. Estuarine, Coastal and Shelf Science 36, 159–181.

Carlson, C.A., Ducklow, H.W., Michaels, A.F., 1994. Annual flux of dissolved organic carbon from the euphotic zone in the northwestern Sargasso Sea. Nature 371, 405–408.

Carpenter, J.H., 1965a. The accuracy of the Winkler method for the dissolved oxygen analysis. Limnology and Oceanography 10, 135–140.

Carpenter, J.H., 1965b. The Chesapeake Bay Institute technique for dissolved oxygen method. Limnology and Oceanography 10, 141–143.

Copin-Montegut, G., Avril, B., 1993. Vertical distribution and temporal variation of dissolved organic carbon in the North-Western Mediterranean Sea. Deep-Sea Research I 40, 1963–1972.

Doval, M.D., Alvarez-Salgado, X.A., Perez, F.F., 2001. Organic matter distributions in the Eastern North Atlantic–Azores front region. Journal of Marine Systems 30, 33–49.

Durrieu de Madron, X., Abassi, A., Heussner, S., Monaco, A., Aloisi, J.-C., Radakovitch, O., Giresse, P., Buscail, R., Kerherve, P., 2000. Particulate matter and organic carbon budgets for the Gulf of Lions (NW Mediterranean). Oceanologica Acta 23 (6), 717–730.

Eppley, R.W., Peterson, B.J., 1979. Particulate organic matter flux and planktonic new production in the deep ocean. Nature 282, 677–680.

Eriksen, C., 1982. Observations of internal wave reflection off sloping bottoms. Journal of Geophysical Research 87 (C1), 525–538.

Eriksen, C., 1985. Implications of ocean bottom reflection for internal wave spectra and mixing. Journal of Physical Oceanography 15, 1145–1156.

Eriksen, C., 1998a. Internal wave reflection and mixing at Fieberling Guyot. Journal of Geophysical Research 103 (C2), 2977–2994.

Eriksen, C., 1998b. Waves, mixing and transports over sloping boundaries. In: Imberger, J. (Ed.), Physical Processes in Lakes and Oceans. Coastal and Estuarine Studies, Vol. 54. American Geophysical Union, pp. 417–440.

Gargett, A.E., 1984. Vertical eddy diffusivity in the ocean interior. Journal of Marine Research 42, 359–393.

Garrett, C., 2000. The dynamic ocean. In: Batchelor, G.K., Moffatt, H.K., Worster, M.G. (Eds.), Perspectives in Fluid Dynamics. Cambridge University Press, Cambridge, UK, pp. 507–556.

Garrett, C., Gilbert, D., 1988. Estimates of vertical mixing by internal waves reflected off a sloping bottom. In: Nihoul, J.C.J., Jamart, B.M. (Eds.), Small-Scale Turbulence and Mixing in the Ocean. Elsevier, New York, pp. 405–424.

Gargett, A.E., Holloway, G., 1984. Dissipation and diffusion by internal wave breaking. Journal of Marine Research 42, 15–27.

Garrett, C.J.R., Munk, W., 1979. Internal waves in the ocean. Annual Review of Fluid Mechanics 11, 339–369.

Gilbert, D., 1990. Theory and observations of internal wave reflection off sloping topography. Ph.D. Thesis, Dalhousie University, Halifax, NS, p. 183.

Gilbert, D., 1993. A search for evidence of critical internal wave reflection on the continental rise and slope off Nova Scotia. Atmosphere-Ocean 31 (1), 99–122.

Gilbert, D., Garrett, C., 1989. Implication for ocean mixing of internal wave scattering off irregular topography. Journal of Physical Oceanography 19, 1716–1728.

Gonella, J., 1972. A rotary component method for analyzing meteorological and oceanographic vector time series. Deep-Sea Research 19, 833–846.

Gregg, M.C., 1998. Estimation and geography of diapycnal mixing in the stratified ocean. In: Imberger, J. (Ed.), Physical Processes in Lakes and Oceans. Coastal and Estuarine Studies, Vol. 54. American Geophysical Union, pp. 305–338.

Hogg, N., Biscaye, P., Gardner, W., Schmitz Jr., W.J., 1982. On the transport and modification of antarctic bottom water in the vema channel. Journal of Marine Research 40 (Suppl.), 231–263.

Jassby, A., Powell, T., 1975. Vertical patterns of eddy diffusion during stratification in Castle Lake, California. Limnology and Oceanography 20, 530–543.

Kunze, E., Toole, J.M., 1997. Tidally driven vorticity, diurnal shear and turbulence atop Fieberling Seamount. Journal of Physical Oceanography 27, 2663–2693.

Ledwell, J.R., Bradkovich, A., 1995. A tracer study of mixing in the Santa Cruz Basin. Journal of Geophysical Research 100 (C10), 20681–20704.

Ledwell, J.R., Hickey, B.M., 1995. Evidence for enhanced boundary mixing in the Santa Monica Basin. Journal of Geophysical Research 100 (C10), 20665–20679.

Lefevre, D., Denis, M., Lambert, C.E., Miquel, J.-C., 1996. Is DOC the main source of organic matter remineralisation in the ocean water column? Journal of Marine Systems 7, 281–291.

Lewis, E.L., Perkin, R.G., 1982. Seasonal mixing processes in an Arctic fjord system. Journal of Physical Oceanography 12, 74–83.

Lien, R.-C., Gregg, M.C., 2001. Observations of turbulence in a tidal beam and across a coastal ridge. Journal of Geophysical Research 106 (C3), 4575–4592.

Lueck, R.G., Mudge, T.D., 1997. Topographically induced mixing around a shallow seamount. Science 276, 1831–1833.

Lykousis, V., Chronis, G., Tselepides, A., Price, B., Theocharis, A., Siokou-Frangou, I., Van Wambeke, F., Danovaro, R., Stavrakakis, S., Duineveld, G., Georgopoulos, D., Ignatiades, L., Souvermezoglou, E., Voutsinou-Taliadouri, F., 2002. Major outputs of the recent multidisciplinary biogeochemical researches undertaken in the Aegean Sea. Journal of Marine Systems 33–34 (C), 313–334.

Martin, J.H., Knauer, G.A., Karl, D.M., Broenkow, W.W., 1987. VERTEX: carbon cycling in the northeast Pacific. Deep-Sea Research 34, 267–285.

Miquel, J.C., Fowler, S.W., La Rosa, J., Buat-Menard, P., 1994. Dynamics of the downward flux of particles and carbon in the open northwestern Mediterranean Sea. Deep-Sea Research I 41, 243–261.

Munk, W.H., 1966. Abyssal recipes. Deep-Sea Research 13, 707–730.

Munk, W.H., 1981. Internal waves and small scale processes. In: Warren, B.A., Wunch, C. (Eds.), Evolution of Physical Oceanography. MIT Press, Cambridge, MA, pp. 264–291.

Nielsen, J.N., 1912. Hydrography of the Mediterranean and adjacent waters. In: Schmidt, J. (Ed.), Report of the Danish Oceanographic Expeditions 1908–1910 to the Mediterranean and adjacent seas. Andr. Fred Host & Son, Copenhagen, pp. 77–192.

Phillips, O.M., 1977. The Dynamics of the Upper Ocean, 2nd Edition. Cambridge University Press, Cambridge, p. 336.

Plakhin, Y.A., 1972. Vertical winter circulation in the Mediterranean. Oceanology 12, 344–351.

Pollak, M.J., 1951. The sources of the deep water of the Eastern Mediterranean. Journal of Marine Research 10, 128–152.

Quay, P.D., Broecker, W.S., Hesslein, R.H., Schindler, D.W., 1980. Vertical diffusion rates determined by tritium tracer experiments in the thermocline and hypolimnion of two lakes. Limnology and Oceanography 25, 201–218.

Roether, W., Well, R., 2001. Oxygen consumption in the Eastern Mediterranean. Deep-Sea Research I 48, 1535–1551.

Siokou-Frangou, I., Bianchi, M., Christaki, U., Christou, E., Giannakourou, A., Gotsis, O., Ignatiades, L., Pagou, K., Pitta, P., Psarra, S., Souvermezoglou, E., Van Wambeke, F., Zervakis, V., 2002. Organic carbon partitioning and carbon flow along a gradient of oligotrophy in the Aegean Sea (Mediterranean Sea). Journal of Marine Systems 33–34, 335–353.

Smethie Jr., W.M., 1980. Estimation of vertical mixing rates in fjords using naturally occurring Radon-22 and salinity as tracers. In: Freeland, H.J., Farmer, D.M., Levings, C.D. (Eds.), Fjord Oceanography. Plenum Press, New York, pp. 241–249.

Souvermezoglou, E., Krasakopoulou, E., 2002. High oxygen consumption rates in the deep layers of the north Aegean Sea. Mediterranean Marine Science 3 (1), 55–64.

Stigebrandt, A., 1976. Vertical diffusion driven by internal waves in a sill Fjord. Journal of Physical Oceanography 6, 486–495.

Stigebrandt, A., Aure, J., 1989. Vertical mixing in Basin waters of Fjords. Journal of Physical Oceanography 19, 917–926.

Stigebrandt, A., Aure, J., Molvaer, J., 1996. Oxygen budget methods to determine the vertical flux of particulate matter with application to the coastal waters off western Scandinavia. Deep-Sea Research II 43 (1), 7–21.

Stommel, H., 1972. Deep winter-time convection in the Western Mediterranean Sea. In: Gordon, A.L. (Ed.), Studies in Physical Oceanography. Gordon and Breach, New York, pp. 207–218.

Svensson, T., 1980. Tracer measurement of mixing in the deep water of a small stratified sill Fjord. In: Freeland, H.J., Farmer, D.M., Levings, C.D. (Eds.), Fjord Oceanography. Plenum Press, New York, pp. 233–240.

Theocharis, A., Georgopoulos, D., 1993. Dense water formation over the Samothraki and Lemnos plateaux in the North Aegean Sea (eastern Mediterranean Sea). Continental Shelf Research 13, 919–939.

Thorpe, S.A., 1987. Current and temperature variability on the continental slope. Philosophical Transactions of the Royal Society of London, Series A 323, 471–485.

Toole, J.M., Ledwell, J.R., Polzin, K.L., Schmitt, R.W., Montgomery, E.T., St. Laurent, L., Owens, W.B., 1997. The Brazil basin tracer release experiment. International WOCE Newsletter 28, 25–28.

Ünlüata, Ü., Oğuz, T., Latif, M.A., Öszoy, E., 1990. On the physical oceanography of Turkish Straits. In: Pratt, L.J. (Ed.), The Physical Oceanography of Sea Straits. Kluwer Academic Publishers, Netherlands, pp. 25–60.

Whitehead Jr., J.A., Worthington, L.V., 1982. The flux and mixing rates of Antarctic bottom water within the North Atlantic. Journal of Geophysical Research 87, 7903–7924.

Wüest, A., van Senden, D.C., Imberger, J., Piepke, G., Gloor, M., 1996. Comparison of diapycnal diffusivity measured by tracer and microstructure techniques. Dynamics of Atmospheres and Oceans 24, 27–39.

Wunsch, C., Hendry, R., 1972. Array measurements of the bottom boundary layer and the internal wave field on the continental slope. Geophysical Fluid Dynamics 4, 101–145.

Zervakis, V., Georgopoulos, D., Drakopoulos, P.G., 2000. The role of the North Aegean Sea in triggering the recent Eastern Mediterranean climatic changes. Journal of Geophysical Research 105 (C11), 26103–26116.

Zodiatis, G., 1994. Advection of the Black Sea water in the North Aegean Sea. The Global Atmosphere and Ocean System 2, 41–60.